Flexible assimilation of human's target for versatile human-robot physical interaction

Article (Accepted Version)

Flexible Assimilation of Human's Target for Versatile Human-robot Physical Interaction

Atsushi Takagi*, Yanan Li*, *Member, IEEE*, and Etienne Burdet, *Member, IEEE*

Abstract—Recent studies on the physical interaction between humans have revealed their ability to read the partner's motion plan and use it to improve one's own control. Inspired by these results, we develop an intention assimilation controller (IAC) that enables a contact robot to estimate the human's virtual target from the interaction force, and combine it with its own target to plan motion. While the virtual target depends on the control gains assumed for the human, we show that this does not affect the stability of the human-robot system, and our novel scheme covers a continuum of interaction behaviours from cooperation to competition. Simulations and experiments illustrate how the IAC can assist the human or compete with them to prevent collisions. We demonstrate the IAC's advantages over related methods, such as faster convergence to a target, guidance with less force, safer obstacle avoidance and a wider range of interaction behaviours.

Index Terms—Physical human-robot interaction, intention assimilation, interaction control.

1 Introduction

In the past decades, "contact robots" have been developed that work in physical interaction with a human, such as for surgery [1] or neuro-rehabilitation [2]. Collaborative robots also physically interact with human workers in order to carry out tasks that are hard or costly to automate such as in construction [3]. In view of the benefits observed in physical interactions between humans [4], [5], [6], [7], [8], [9], [10], [11], [12], a contact robot knowing the human operator's motion intention could improve the interaction and performance. Extensive effort has been devoted to developing estimation of the human intention during physical interaction (see [13] for a review). In [14], [15], [16], [17], [18], a discrete set of possible goals, states or motion primitives are prescribed and human motion intention is defined as one of them. These approaches require prior knowledge of a task and the estimated human motion intention is subject to various limitations. In [19], [20], [21], human motion intention is estimated based on various computational models of human behaviours, which need to be trained with offline demonstrations and data. In [22], [23], [24], [25], [26], human motion intention is defined as the human position in the future and thus can provide continuous prediction of human movement. These approaches are usually based on a model of human movement whose parameters are required to be estimated accurately. While the approach in this paper uses a similar definition of human intention i.e., continuously predicted future position, it does not require an accurate estimate of the "real" human intention, and thus relaxes the strong assumptions about the human model or their movement.

When the human's intention can be estimated, the robot control can be designed to either assist the human's movement [27], [28], [29] or resist it [30], [31]. While a leader-follower framework is widely adopted to allow a human user to guide a robot, researches have been focused on making the robot's following proactive using estimated human intention [32]. However, robots do not always have to follow or even cooperate with a human. Shared control between them can be benefited by adjusting their roles according to changing task objectives and their respective advantages [33], [34], [35]. Our previous studies [36], [37], [38] have shown how robots without a predefined role can adapt their control to the human's behaviour in order to improve task performance and minimize effort. A systematic taxonomy of roles to analyse and implement shared control between a robot and the human has been proposed in [39]. Furthermore, an antagonistic robot may be desirable in many scenarios [40]. For instance, rehabilitation robots may deliberately challenge the trainee by amplifying their movement errors to improve the outcomes of physical therapy [31]. In robot-aided surgery, it may be desirable for the teleoperated robot to overpower a surgeon's action to avoid slicing a vital organ that the surgeon overlooked. In this paper we develop a unified framework that can continuously change the robot's interactive behavior from assistance to competition, and which does not rely on an accurate estimate of the human's control unlike [38].

The major differences between the intention assimilation controller (IAC) introduced in this paper and other interaction schemes in the literature are threefold. First, the IAC does not depend on an accurate estimate of the human's

- *This research was supported in part by the Royal Society grant IES/R3/193136, the UK EPSRC grants EP/NO29003/1, EP/T006951/1, EP/R026092/1, as well as by the European Commission grants H2020 PH-CODING (FETOPEN 829186), INTUITIVE (ITN 861166), CONBOTS (ICT 871803) and REHYB (ICT 871767).*

- ** The first two authors contributed equally to the work.*

- *The authors are or were with the Department of Bioengineering, Imperial College of Science, Technology and Medicine, SW7 2AZ London, UK. E-mail: eburdet@ic.ac.uk*
- *A. Takagi is with the NTT Communication Science Laboratories, Kanagawa, 243-0198, Japan.*
- *Y. Li is with the School of Engineering and Informatics, University of Sussex, Brighton, BN1 9RH, UK. Email: yl557@sussex.ac.uk.*

control, which cannot be identified on simple trajectories [10], [38], and may require strong assumptions about the human model or their movement [22], [23], [24], [25], [26], or additional sensing modalities not equipped by most robots [41]. Second, the IAC provides a continuous spectrum of interaction behaviours from assistance to competition that is determined by an open parameter. In comparison, other schemes focus either on cooperation [7], [33], [37], [42], [43] or competition [30], [31], or switch between these two extreme behaviours. Third, the IAC relies on the prediction of the human's target trajectory (not merely on their current state as in [33]) to determine its behaviour, so it can provide motion guidance with less force and safer obstacle avoidance.

Sections II and III describe how the IAC uses a prediction of the human's virtual target trajectory to determine the robot's behaviour. Section IV examines the stability of the human-robot system in the continuous spectrum of behaviours from cooperation to competition. Section V demonstrates the flexibility offered by the virtual target, showcasing some interaction scenarios alongside a comparison with existing interaction schemes. Through simulations and experiments on a robotic interface, we first test a scenario where the IAC interacts with a human to reduce their effort during cooperative manipulation. We then examine a scenario where an antagonistic IAC competes against the human to prevent a collision with an unforeseen obstacle.

2 HUMAN-ROBOT SYSTEM DYNAMICS

We consider a task where a robot gripper and a human hand manipulate a rigid object together. For simplicity, we assume that there is no relative motion between the robot gripper, human hand and object, and the object is a point mass. Considering only linear motion, the common object manipulation has dynamics

$$M_o\,\ddot{x} \;+\; G_o = \; f + u_h \tag{1}$$

where $x(t) \in \mathbb{R}^3$ is the object's position, $f(t)$ and $u_h(t)$ are forces applied on the object by the robot and the human, respectively. $M_o \in \mathbb{R}^{3\times3}$ is the mass matrix and $G_o \in \mathbb{R}^3$ is the gravitational force, which can be expanded as follows:

$$M_o = \; m_o \mathbb{1}_3\,, \quad G_o = \begin{bmatrix} 0 \\ 0 \\ -m_o\, g \end{bmatrix} \tag{2}$$

where m_o is the object's mass and $\mathbb{1}_3$ the 3×3 identity matrix.

The dynamics of the $n-$degrees-of-freedom robot are described in joint space as

$$M_q(q)\,\ddot{q} + C_q(q,\dot{q})\,\dot{q} + G_q(q) = \tau_q - J^T(q) f \tag{3}$$

where $q \in \mathbb{R}^n$ is the robot's joint coordinate and $\tau_q \in \mathbb{R}^n$ is the control input. $J(q) \in \mathbb{R}^{3\times n}$ is the Jacobian matrix. $M(q) \in \mathbb{R}^{n\times n}$ is the robot's inertia matrix, $C(q,\dot{q})\dot{q} \in \mathbb{R}^n$ the Coriolis and centrifugal torque, $G(q) \in \mathbb{R}^n$ the gravitational torque. The dynamics in (3) can be transformed to the robot's operational space:

$$M_r \ddot{x} + C_r \dot{x} + G_r = u - f \tag{4}$$

where the robot's position x is the same as the object's position in Eq. (1), and $u = J^{\dagger T}(q)\tau_q$ is the robot's control input with $J^\dagger(q)$ as the pseudo inverse of $J(q)$. M_r, C_r and G_r are the robot's inertia, Coriolis, centrifugal and gravitational matrices in the operational space, which are computed as

$$\begin{aligned} M_r &= J^{\dagger T}(q)\, M(q)\, J^\dagger(q) \\ C_r &= J^{\dagger T}(q)\,[C(q,\dot{q}) - M(q)\, J^\dagger(q)\,\dot{J}(q)]\, J^\dagger(q) \\ G_r &= J^{\dagger T}(q)\, G(q)\,. \end{aligned} \tag{5}$$

From Eqs. (1) and (4), we obtain the combined dynamics of the object and the robot as

$$\begin{aligned} &M\ddot{x} + C\dot{x} + G = u + u_h\,, \\ &M \equiv M_o + M_r\,,\;\; G \equiv G_o + G_r\,, C \equiv C_r\,. \end{aligned} \tag{6}$$

where the arguments of M, C and G are omitted for convenience of analysis. We note that the inertia matrix M is symmetric and positive definite and $2C - \dot{M}$ is a skew-symmetric matrix if C is in the Christoffel form [44] thus

$$\rho^T(2C - \dot{M})\rho \;=\; 0 \quad \forall \rho \in \mathbb{R}^3. \tag{7}$$

This property will be used in later stability analysis.

It is assumed that the robot has information about its local environment and has measurement of the system position, velocity and the human force, all subject to measurement noise. Therefore, we use a robot controller with gravity compensation and linear feedback

$$u = \; G - L_1(x - \tau) - L_2\,\dot{x} \tag{8}$$

where τ is the robot's target position, L_1 and L_2 are the gains corresponding to position error and velocity, which can be interpreted as stiffness and viscosity matrices [45]. The gravity matrix G can be identified (beforehand) using adaptive control [46].

Furthermore, (assuming that the human arm dynamics are compensated separately,) we model the force that the human hand applies to the object as

$$u_h = -L_{h,1}(x - \tau_h) - L_{h,2}\,\dot{x} \tag{9}$$

where $L_{h,1}$ and $L_{h,2}$ are the human control gains and τ_h is the human's target position. This model indicates how the human aims to move to their target position by using a feedback controller, and it will be used for the robot's estimation of the human's target. Therefore, the proposed method in this paper is subject to the validity of this model, as will be verified in experiments with human participants.

By substituting Eqs. (8) and (9) into Eq. (6), we obtain the closed-loop system dynamics

$$M\ddot{x} + (C + L_2 + L_{h,2})\dot{x} + (L_1 + L_{h,1})x = L_1\tau + L_{h,1}\tau_h \tag{10}$$

As the inertia matrix and the human's controller gains $L_{h,1}$ and $L_{h,2}$ are assumed to be positive definite, the closed-loop system Eq. (10) is stable if L_1 and L_2 are chosen such that $C + L_2 + L_{h,2}$ and $L_1 + L_{h,1}$ are positive definite [47].

3 ASSIMILATION OF THE HUMAN'S INTENTION

3.1 Estimation of human's target

To realize various interaction behaviours, the robot needs to know the human's target position τ_h. Here, we assume that the human's control input u_h is measured using a force sensor subject to measurement noise. To simplify the notation, we describe the estimation of the human's target in one dimension, which can be extended to 3 dimensions.

Can τ_h be estimated using u_h? According to Eq. (9), τ_h can be calculated if the human's control gains $L_{h,1}$ and $L_{h,2}$ are known. It is possible to simultaneously identify the human target τ_h and control gains $L_{h,1}$ and $L_{h,2}$, but this requires a sufficiently "rich" trajectory x meeting the persistent excitation (PE) condition [48]. However, simple tasks do not involve such a rich trajectory [10]. Therefore, we want to develop an alternative approach that does not require an estimation of the human's control gains, by using the "virtual" target that results from assuming arbitrary values for these gains.

We notice that the human's effect on the system dynamics is determined solely through u_h, no matter what internal model it is based on. Therefore, the calculation of the virtual target τ_h^v would be effective in assessing the human's effect on the system dynamics if it satisfies

$$u_h = -L_{h,1}^v(x - \tau_h^v) - L_{h,2}^v \dot{x}\,. \tag{11}$$

How should the virtual human control gains $L_{h,1}^v$ and $L_{h,2}^v$ be selected? They could be estimated from the neuromechanics of each user [49]. Alternatively, one may use some average values measured from many people, or the same values as the robot's controller gains i.e., $L_{h,1}^v \equiv L_1, L_{h,2}^v \equiv L_2$.

In order to estimate τ_h^v, we parameterize it using the internal model

$$\tau_h^v = \theta^T \phi \tag{12}$$

where θ^T is the transpose of the parameter vector that determines τ_h^v and

$$\phi = [1, t, \ldots, t^m]^T \tag{13}$$

with m the order of the virtual target τ_h^v. This model means that the virtual target can be any time-dependent trajectory. For example, $\tau_h^v = p$ indicates a target position at p and $\tau_h^v = p + vt$ a trajectory starting at position p and moving with velocity v.

By using the state vector $\varphi \equiv [x, \dot{x}, \theta^T, u_h]^T$, we combine the system dynamics in Eq. (6) and the above internal model to obtain an extended model

$$\dot{\varphi} = \begin{bmatrix} \dot{x} \\ \ddot{x} \\ 0 \\ \dot{u}_h \end{bmatrix} + \nu \tag{14}$$

where $\nu \in N(0, E[\nu\,\nu^T])$ is system noise.

By assuming that the robot can measure its endpoint position and velocity as well as the interaction force with the human using suitable sensors, we have the robot's measurement vector

$$z \equiv \begin{bmatrix} x \\ \dot{x} \\ u_h \end{bmatrix} + \mu \equiv H\varphi + \mu\,, \quad H \equiv \begin{bmatrix} 1 & 1 & 0 & 1 \end{bmatrix} \tag{15}$$

where $\mu \in N(0, E[\mu\,\mu^T])$ is measurement noise.

Since τ_h^v and thus θ in Eq. (12) are unknown, the following system observer is developed to compute the robot's estimate of the extended state

$$\begin{aligned} \dot{\hat{\varphi}} &= \begin{bmatrix} \dot{\hat{x}} \\ \ddot{\hat{x}} \\ 0 \\ \dot{\hat{u}}_h \end{bmatrix} + K(z - \hat{z}) \\ \hat{u}_h &= -L_{h,1}^v(x - \hat{\tau}_h) - L_{h,2}^v \dot{x} \\ \hat{z} &= H\hat{\varphi},\ \hat{\tau}_h = \hat{\theta}^T \phi \end{aligned} \tag{16}$$

where $\hat{}$ stands for the estimate of the corresponding variable and the linear quadratic estimation (LQE) gain K can be calculated as

$$K = PH^T R^{-1} \tag{17}$$

P is a positive definite matrix obtained by solving the Riccati equation

$$PA^T + AP - PH^T R^{-1} HP + Q = \dot{P}\,, \tag{18}$$

with the noise covariance matrices $Q \equiv E[\nu\nu^T]$ and $R \equiv E[\mu\mu^T]$. A is the system matrix obtained by bringing Eq. (14) in the form

$$\begin{aligned} &\dot{\varphi} = A\,\varphi + B(u - G) + \nu\,,\ \varphi = \begin{bmatrix} x \\ \dot{x} \\ \theta \\ u_h \end{bmatrix},\ B = \begin{bmatrix} 0 \\ M^{-1} \\ 0 \\ L_{h,2}^v M^{-1} \end{bmatrix}, \\ &A = \begin{bmatrix} 0 & 1 & 0 & 0 \\ 0 & -M^{-1}C & 0 & M^{-1} \\ 0 & 0 & 0 & 0 \\ 0 & -L_{h,1}^v + L_{h,2}^v M^{-1} C & L_{h,1}^v \dot{\phi} & -L_{h,2}^v M^{-1} \end{bmatrix} \end{aligned} \tag{19}$$

where the second row is from Eq. (6), and the last row is obtained by differentiating Eq. (11) and substituting Eqs. (6) and (12). With A and H in Eq. (15), it is evident that all states are observable with the exception of θ.

3.2 Intention Assimilation Robot

Eq. (10) shows that the actual position x is determined by the robot's and the human's target position τ and τ_h, respectively. Therefore, we argue that the interaction between the human and robot can be specified by the relationship between τ and τ_h. For example, $\tau = \tau_h$ corresponds to assistance where the robot uses the human's virtual target, and $\tau = \tau_r$ where the robot follows its original target τ_r. Furthermore, $\tau = 2\tau_r - \tau_h$ corresponds to "antagonism" where the robot imposes its own target by eliminating the human's target from the system. These examples can be viewed as special cases of interaction defined along a continuous spectrum of behaviours realized by assimilating the human's target.

To induce a general interaction behaviour, the robot's target position is designed based on the estimated human's target, as

$$\tau = \lambda\,\tau_r + (1 - \lambda)\,\hat{\tau}_h \tag{20}$$

where the weight $\lambda \geq 0$ determines the agonistic or antagonistic behaviour of the robot (Fig.1). In particular, $\lambda = 0$ is assistive behaviour where the robot mirrors

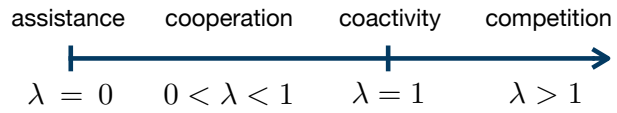

Fig. 1: Continuum of roles defined by the IAC. The weight $\lambda \geq 0$ determines the agonistic or antagonistic behaviour of the robot as described in Section 3.2.

the human's control inputs. The robot is cooperative with $0 < \lambda < 1$ as the IAC considers both the human's and its own target. When $\lambda = 1$, the robot displays neutral behaviour by following its own reference τ_r while ignoring the interaction force arising from the human's control input. Lastly, $\lambda > 1$ is antagonistic behaviour where the robot opposes the human's control inputs. While the selection of λ value is task-dependent, we will show how it affects the robot behaviour in simulations and in experiments with human participants.

This approach is related to the concept of homotopy switching between the leader and follower roles [33], but involves a broader spectrum including various levels of opposition, where the human's control inputs are opposed to counteract their effect on the system. Another key difference is that the IAC uses the human's target position, so it can predict the human's near future behavior, while the homotopy switching in [33] uses the human's current position. These aspects will be illustrated in the simulation and experimental results. Our target-based description of human-robot interaction is also related to the roles taxonomy of [39] which defines an interaction behavior based on weights in each agent's cost function, but our scheme can be directly implemented on position-controlled robots.

4 Stability Analysis

Will the virtual target estimation and its use in the robot's controller destabilize the human-robot system? To address this question we analyse the transient performance of the human-robot system and its closed-loop stability.

From the second equation in the system observer Eq. (16), the estimated human's target is

$$\hat{\tau}_h = x + \frac{\hat{u}_h + L^v_{h,2}\,\dot{x}}{L^v_{h,1}} \tag{21}$$

The robot controller of Eq. (8) then becomes

$$\begin{aligned} u &= G(x) - L_1[x - \lambda\tau_r - (1-\lambda)\hat{\tau}_h] - L_2\dot{x} \qquad (22)\\ &= G(x) - L_1\left[x - \lambda\tau_r - (1-\lambda)\left(x + \frac{\hat{u}_h + L^v_{h,2}\dot{x}}{L^v_{h,1}}\right)\right] - L_2\dot{x} \\ &= G(x) + \lambda L_1(\tau_r - x) + \left[\frac{L_1 L^v_{h,2}}{L^v_{h,1}}(1-\lambda) - L_2\right]\dot{x} \\ &\quad + \frac{L_1}{L^v_{h,1}}(1-\lambda)\,\hat{u}_h \end{aligned}$$

Substituting this robot controller into Eq. (6), we obtain

$$\begin{aligned} &M\ddot{x} + \left[C + L_2 - \frac{L_1 L^v_{h,2}}{L^v_{h,1}}(1-\lambda)\right]\dot{x} + \lambda L_1\, x \qquad (23)\\ &= \lambda L_1\tau_r + \frac{L_1}{L^v_{h,1}}(1-\lambda)\hat{u}_h + u_h \\ &= \lambda L_1\tau_r + \left[\frac{L_1}{L^v_{h,1}}(1-\lambda) + 1\right]u_h + \frac{L_1}{L^v_{h,1}}(1-\lambda)\tilde{u}_h \end{aligned}$$

where $\tilde{(\cdot)} = \hat{(\cdot)} - (\cdot)$. By defining $\bar{\lambda} = \frac{L_1}{L^v_{h,1}}(1-\lambda)$ and substituting the human's controller of Eq. (9) into the above equation, we obtain

$$\begin{aligned} &M\ddot{x} + [C + L_2 - \bar{\lambda}L^v_{h,2} + (\bar{\lambda}+1)L_{h,2}]\,\dot{x} \qquad (24)\\ &\quad + [\lambda L_1 + (\bar{\lambda}+1)L_{h,1}]x \\ &= \lambda L_1\tau_r + (\bar{\lambda}+1)\,L_{h,1}\,\tau_h \;+\; \bar{\lambda}\tilde{u}_h \end{aligned}$$

With the above equation, we can analyze the effects of τ_r and τ_h on the system dynamics. Considering the steady-state position

$$x_{ss} \equiv \frac{\lambda L_1\tau_r + (\bar{\lambda}+1)\,L_{h,1}\,\tau_h}{\lambda L_1 + (\bar{\lambda}+1)L_{h,1}} \tag{25}$$

defined by $\dot{x} = \ddot{x} \equiv 0$ yields

$$\begin{aligned} &M\ddot{x} + [C + L_2 - \bar{\lambda}L^v_{h,2} + (\bar{\lambda}+1)L_{h,2}]\,\dot{x} \\ &+ [\lambda L_1 + (\bar{\lambda}+1)L_{h,1}](x - x_{ss}) = \bar{\lambda}\,\tilde{u}_h\,. \qquad (26) \end{aligned}$$

By defining

$$\begin{aligned} \bar{L}_1 &\equiv \lambda L_1 + (\bar{\lambda}+1)L_{h,1}\,, \\ \bar{L}_2 &\equiv L_2 - \bar{\lambda}L^v_{h,2} + (\bar{\lambda}+1)L_{h,2}\,, \end{aligned} \tag{27}$$

we rewrite Eq. (26) as

$$M\ddot{x} + (C + \bar{L}_2)\,\dot{x} + \bar{L}_1(x - x_{ss}) = \bar{\lambda}\,\tilde{u}_h\,. \tag{28}$$

which indicates that the position error $x - x_{ss}$ would disappear if the estimation error of the human force is $\tilde{u}_h = 0$. Therefore, we need to check how $\tilde{u}_h$ evolves with the developed observer.

According to the system dynamics in state-space form in Eq. (19) and its observer in Eq. (16), we have

$$\dot{\tilde{\varphi}} = (A - KH)\,\tilde{\varphi} + \varepsilon\,, \quad \varepsilon \equiv -\nu - K\mu\,. \tag{29}$$

By defining $\xi \equiv [x - x_{ss}, \dot{x}, \tilde{\varphi}^T]^T$ and combining Eqs. (28) and (29), we obtain

$$\begin{aligned} \dot{\xi} &= \bar{A}\,\xi + \bar{B}\,\varepsilon, \qquad (30)\\ \bar{A} &= \begin{bmatrix} 0 & 1 & 0 \\ -M^{-1}\bar{L}_1 & -M^{-1}(C + \bar{L}_2) & M^{-1}\bar{\lambda}\bar{H} \\ 0 & 0 & A - KH \end{bmatrix}, \\ \bar{B} &= \begin{bmatrix} 0 \\ 0 \\ \mathbb{1} \end{bmatrix},\ \bar{H} = \begin{bmatrix} 0 \\ 0 \\ 0 \\ 1 \end{bmatrix} \end{aligned}$$

Eq. (30) is the combined system including the system dynamics and the observer, which can be used to analyze the system's transient performance. Solving Eq. (30) yields

$$\xi = e^{\bar{A}t}\xi(0) + \int_0^t e^{\bar{A}(t-\tau)}\bar{B}\,\varepsilon(s)\,\mathrm{d}s \tag{31}$$

with the expected value

$$E[\xi] = e^{\bar{A}t}E[\xi(0)] + \int_0^t e^{\bar{A}(t-\tau)}\bar{B}\,E[\varepsilon(s)]\,\mathrm{d}s \tag{32}$$

To study the stability of the combined system in Eq. (30), we can compute the eigenvalues of $\bar{A}$, which are the solutions y of the characteristic equation

$$[yI-(A-KH)][My^2+(C+\bar{L}_2)y+\bar{L}_1] = 0\,. \tag{33}$$

We note that the eigenvalues y are determined from the dynamics in Eq. (28) and the estimation error dynamics in Eq. (29), but not from their coupling term $M^{-1}\bar{\lambda}\bar{H}$, which thus does not affect the system stability. Therefore, the stability of $\bar{A}$ is ensured if the following two systems are stable:

$$M\ddot{x} + (C+\bar{L}_2)\,\dot{x} + \bar{L}_1(x-x_{ss}) = 0 \tag{34}$$

$$\dot{\tilde{\varphi}} = (A-KH)\tilde{\varphi} \tag{35}$$

In the following, we test the stability of the above two systems respectively using Lyapunov theory.

We first prove the stability of the first system by considering the Lyapunov function candidate

$$V_1 = \frac{1}{2}M\dot{x}^2 + \frac{1}{2}\bar{L}_1(x-x_{ss})^2, \quad \bar{L}_1 > 0\,. \tag{36}$$

with time derivative

$$\dot{V}_1 = \dot{x}\left(\frac{1}{2}\dot{M}\dot{x} + M\ddot{x}\right) + \bar{L}_1(x-x_{ss})\dot{x}\,. \tag{37}$$

Using Eqs. (7) and (34) we obtain

$$\dot{V}_1 = \dot{x}(C\dot{x}+M\ddot{x}) + \bar{L}_1(x-x_{ss})\dot{x} = -\bar{L}_2\,\dot{x}^2 \le 0 \tag{38}$$

indicating that the system in Eq. (34) is stable when $\bar{L}_2 > 0$.

We then prove the stability of Eq. (35) by considering the Lyapunov function candidate

$$V_2 = \tilde{\varphi}^T P_v\,\tilde{\varphi}\,, \quad P_v \equiv P^{-1}\,. \tag{39}$$

From the Riccati equation in Eq. (18) we get

$$P_vA + A^TP_v - H^TR^{-1}H + P_vQP_v = -\dot{P}_v\,. \tag{40}$$

The time derivative of V_2 is

$$\dot{V}_2 = \tilde{\varphi}^T\dot{P}_v\tilde{\varphi} + 2\,\tilde{\varphi}^TP_v\dot{\tilde{\varphi}}\,. \tag{41}$$

According to the definition of K in Eqs. (17) and (35), we have

$$\dot{\tilde{\varphi}} = (A-PH^TR^{-1}H)\,\tilde{\varphi}\,. \tag{42}$$

It follows

$$2\,\tilde{\varphi}^TP_v\dot{\tilde{\varphi}} = \tilde{\varphi}^T(P_vA + A^TP_v - 2H^TR^{-1}H)\tilde{\varphi}\,. \tag{43}$$

With Eqs. (40) and (43), we then obtain

$$\dot{V}_2 = -(P_v\tilde{\varphi})^TQ\,P_v\tilde{\varphi} - (H\tilde{\varphi})^TR^{-1}H\tilde{\varphi} \le 0 \tag{44}$$

which indicates that the system in Eq. (35) is stable. Therefore the estimation error of observable states $[\tilde{x},\dot{\tilde{x}},\tilde{u}_h]$ is asymptotically stable (except $\tilde{\theta}$ corresponding to an eigenvalue of $\bar{A}$ at 0).

Therefore, the eigenvalues of $\bar{A}$ are all negative, except 0 corresponding to the unobservable state θ. Correspondingly, the first term in Eq. (32) vanishes for $t\to\infty$, except $E[\tilde{\theta}(0)]$ which is bounded. In the second term, $E[\varepsilon(s)] = 0$ because $E[\nu] = E[\mu] = 0$. Therefore, according to the definition of the state $\xi = [x-x_{ss},\dot{x},\tilde{\varphi}^T]^T$ with $\tilde{\varphi} = [\tilde{x},\dot{\tilde{x}},\tilde{\theta}^T,\tilde{u}_h]^T$, we have $E[\dot{x}]\to 0$, $E[x-x_{ss}]\to 0$, $E[\tilde{x}]\to 0$, $E[\dot{\tilde{x}}]\to 0$, $E[\tilde{u}_h]\to 0$ for $t\to\infty$.

Remark 1. The condition $\bar{L}_1 > 0$, $\bar{L}_2 > 0$ can be satisfied by choosing L_1, L_2, $L^v_{h,1}$, $L^v_{h,2}$ according to the definitions of $\bar{L}_1$, $\bar{L}_2$ in Eq. (27). As an example, we explain here how this can be done in the case when $L_1 \equiv L^v_{h,1}$, $L_2 \equiv L^v_{h,2}$ and thus

$$\begin{aligned}\bar{L}_1 &\equiv \lambda L_1 + (2-\lambda)L_{h,1}\,,\\ \bar{L}_2 &\equiv \lambda L_2 + (2-\lambda)L_{h,2}\,,\end{aligned} \tag{45}$$

Here, $\bar{L}_1 > 0$ and $\bar{L}_2 > 0$ are valid for $0 \le \lambda \le 2$. For assistance, $\lambda = 0$ leads to $x_{ss} = \hat{\tau}_h$ as in Eq. (25). For a special case of competition, $\lambda = 2$ leads to $x_{ss} = \tau_r$. If $\lambda > 2$ competition may cause system instability as may be expected. In this case, we can effectively set the robot's gains to be greater than the human's, i.e. $L_1 > L_{h1}$ and $L_2 > L_{h2}$ to maintain stability (assuming that the human has bounded control gains).

5 Simulations and Experiments

We carried out simulations and experiments with four human participants (33±1 years old, all male and with prior experience using haptic interfaces) in order to test the properties of the IAC, illustrate two applications and compare its performance with other interaction schemes. The participants were asked to trace a circular path at a constant velocity.

5.1 Methods

To demonstrate the algorithm's ability to generate cooperative and competitive behaviours, we first simulated scenarios of human-robot interaction where the robot adapts its behaviour to a simulated human partner with fixed parameters. In the simulations, the mass of each agent was set to 1 kg such that the simulated system's state, composed of the position x and velocity $\dot{x}$, evolved according to $\ddot{x} = u + u_h$, which was discretized with a step-size of $\mathrm{dt} \equiv 0.01$ s. The Kalman filter's noise covariance matrices for Eq. (18) were

$$Q \equiv \begin{bmatrix}0.001 & 0\\ 0 & 0.001\end{bmatrix},\ R \equiv 0.001,\ P \equiv \begin{bmatrix}1 & 0\\ 0 & 1\end{bmatrix} \tag{46}$$

where only the force measurement is observed as the states x and $\dot{x}$ are assumed to be known. Eq. (11) is used to compute the control command to move the robot while its reference trajectory is given by Eq. (20) using the estimated virtual target from Eq. (12) with a zeroth order internal model. The human control gains are set as $L_h \equiv [30\,\mathrm{N/m},\ 8\,\mathrm{Ns/m}]$ for all subsequent simulations (units are dropped henceforth).

Then, we implemented the IAC on the KINARM (from BKIN Technologies). The participant held onto the handle of this planar robotic interface. The KINARM can measure the forces applied by the participant using a six-axis ATI Mini45 force sensor mounted above the handle of the interface. The position of the participant's hand was displayed as a white cursor on a monitor which was viewed from a film mirror

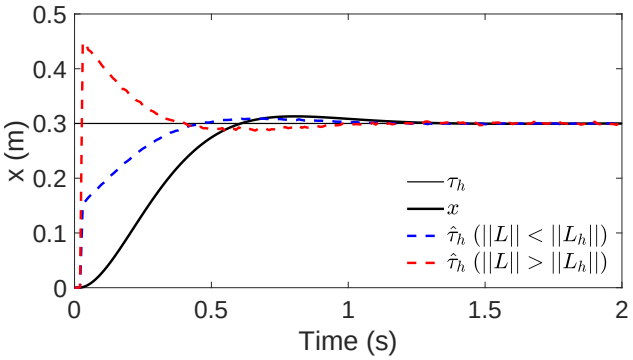

Fig. 2: Simulation of the effect of various control gains assumed for the human. The human's target is estimated using two different values of L, where the estimated gain is either smaller (dotted blue trace) or greater (dotted red trace) than the actual gain L_h.

placed above the KINARM's workspace (Figure 5). In the experiment, the Kalman filter's noise covariance matrices were

$$Q \equiv \begin{bmatrix} 1 & 0 \\ 0 & 1 \end{bmatrix}, \quad R \equiv 0.1\ , \quad P \equiv \begin{bmatrix} 1 & 0 \\ 0 & 1 \end{bmatrix}. \tag{47}$$

5.2 Robustness of the estimation of the human's virtual target

To demonstrate the ability to estimate the human's virtual target, we simulate a human that reaches a static target $\tau_h \equiv 0.3$ m in an LQR-like manner while the robot's control input u is 0. Figure 2 shows the simulation where the robot estimates the human's target using incorrect gains. When the robot's gain is smaller than the simulated human's e.g., $L \equiv [22, 7]$, the estimated simulated human's target is overshot. If the robot assumes a larger gain than the simulated human's, $L \equiv [52, 10]$, the target is first undershot by its estimation, which then again converges to it. It should be noted that the estimated target $\hat{\tau}_h$, though initially incorrect, converges to τ_h, which can be only achieved when either $\lambda = 0$ or $u = 0$.

5.3 Implementation of different interaction strategies

Here, we examine in simulation how the IAC can implement different interactive behaviours. We use $\lambda = \{0,1,2\}$ to illustrate how the robot is cooperating with, ignoring or competing against the simulated human, respectively. The simulated human with the target τ_h has $\lambda_h = 1$. The IAC's original target is τ_r. The cooperative IAC with $\lambda = 0$ discards its own target τ_r to help the simulated human reach their target (green trace of Figure 3). More generally, when $\lambda < 1$ and the IAC has a different target as the simulated human, the IAC will negotiate a compromise between the two targets. In the case of coactivity, when the IAC ignores the simulated human partner using $\lambda = 1$, the position at which the system will stabilize will depend on their relative strengths. The stronger IAC biases the position towards τ_r (black trace of Figure 3). The competitive IAC with $\lambda = 2$ eliminates the simulated human's effect on the dynamics of the system and the system position eventually converges to the IAC's target τ_r (red trace of Figure 3).

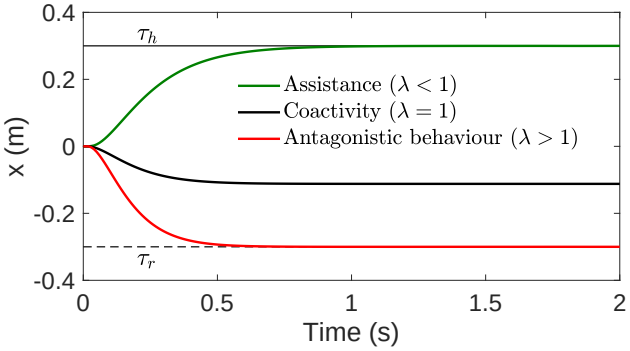

Fig. 3: Simulation showing the different interaction strategies available to the IAC. The simulated human and the robot have different targets at $\tau_h = 0.3$m and $\tau_r = -0.3$m. A constant $\lambda_h = 1$ is used to best illustrate the robot's behaviour for different values of λ. $\lambda = 1$ corresponds to coactivity, where the simulated human and robot both attempt to reach their reference target whilst ignoring the partner (black trace). With $\lambda = 0$ the robot cooperates by attempting to reach the simulated human's target, effectively mirroring their control input (green trace). With $\lambda = 2$ the robot competes with the simulated human to impose and reach its own target.

5.4 Cooperative IAC's ability to assist performance

The behaviour of a cooperative IAC is investigated in this section, first in simulation then in an experiment. In the simulation, the interaction between a simulated human with $\lambda_h = 1$ and an IAC with $\lambda = 0$ is compared to a standard leader-follower paradigm [27], [28], [32], wherein the robot tries to follow and stay at the simulated human's position, and to the simulated human reaching its target $\tau_h = 0.3$ without assistance (Figure 4). In the leader-follower paradigm, if the robot follows a simulated human and their positions are the same, its control input is $u = -L_2\,\dot{x}$, acting like a brake, causing the simulated human to exert the most effort. The IAC with $\lambda = 0$ assists the simulated human such that the human's control inputs are mirrored, helping them to reach the target faster than without interaction and with less effort.

In the experiment, we asked four participants to trace a circular path of radius 0.15 m with a constant velocity for 6 seconds (Figure 5A). A representative trial is shown in Figure 5B. Five different assistants were tested in blocks of 5 trials: compliant IAC ($L_h^{(c)} \equiv [25,6]$), medium IAC ($L_h^{(m)} \equiv [100,10]$), stiff IAC ($L_h^{(s)} \equiv [400,24]$), the homotopy framework of [33], and no assistance. The compliant gains were the lowest possible gains that kept the estimated human's target within the workspace of the robot. The stiff gains were bounded for the safety of the human participant. The medium gain was set in between these two.

The homotopy framework exerts a force corresponding to the weighted sum of the robot's control input u and the human's input u_h

$$u = \lambda\, u + (1-\lambda)\, u_h\,, \quad 0 \le \lambda \le 1\,. \tag{48}$$

The three IACs were cooperative with $\lambda = 0$.

The group mean tangential velocity $||v||$ (Figure 5C) and the group mean tangential force $||F||$ (Figure 5D) were calculated for each type of assistance. While $||v||$ was comparable for all conditions, $||F||$ was significantly lower with the cooperative IACs and with the homotopy framework with respect to no assistance. Thus, in terms of cooperative behavior, the IAC performs similarly to the homotopy framework.

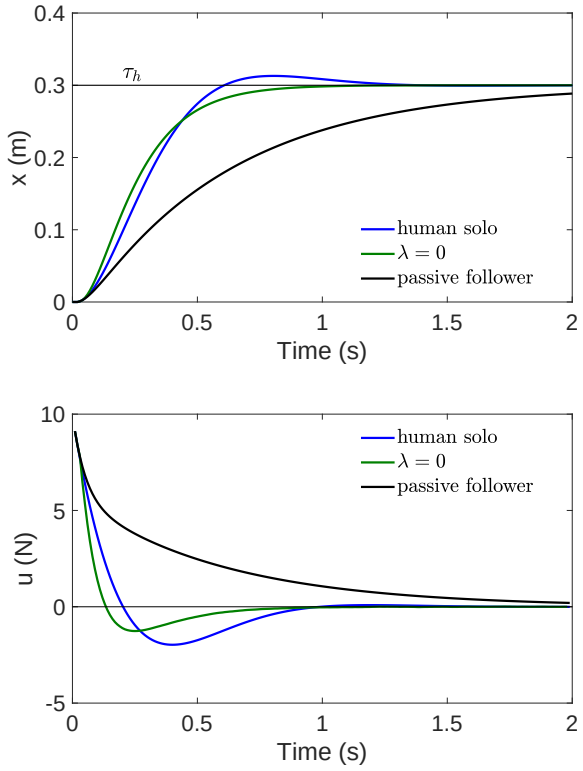

Fig. 4: Simulation comparing the IAC with other cooperative strategies. The simulated human's effort decreases when $\lambda = 0$ in comparison to a passive follower or a simulated human doing the task alone.

5.5 Competing IAC for robust collision avoidance

When should a robot display a competitive behaviour with the human? In teleoperation, there may be instances where the human operator does not see an obstacle and may collide with it e.g., in robot-assisted surgery. If the robot has the ability to sense obstacles, it could compete to prevent the human operator from a collision. This scenario is simulated with an IAC that assumes that either the simulated human's control gains are greater ($\|L_h^v\| > \|L_h\|$) or less ($\|L_h^v\| < \|L_h\|$) than they actually are (Figure 6). A discrepancy between τ_h and τ_h^v occurs in both cases, but flexible collision avoidance behaviour can still be implemented. The

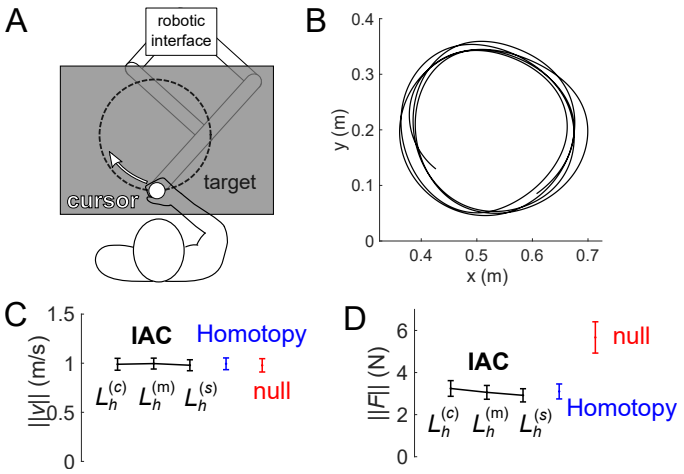

Fig. 5: Experiment comparing assistance with the IAC and with the homotopy framework to carry out circular movements at constant speed. (A) Schematic of the task. Each assistance modality was tested in a block of 5 trials, each lasting 6 seconds. (B) Representative cursor trajectory from a trial with the compliant cooperative IAC. (C) Group mean tangential velocity $||v||$ (error bars signify one standard error) was comparable for the compliant IAC $L_h^{(c)}$, medium IAC $L_h^{(m)}$ or stiff IAC $L_h^{(s)}$ (all in black), the homotopy framework (blue), and no assistance (red). (D) The group mean tangential force $||F||$ was high without assistance, and comparable for all IACs and the homotopy framework.

IAC's collision avoidance capability is compared against the homotopy framework [33].

The simulated human's target τ_h (thin black trace in Figure 6) is triangular, and breeches the wall when $0.5 < t < 1.5$ s. When the IAC's estimate of the simulated human target $\hat{\tau}_h$ (dashed and dotted black traces) is far from the wall, it foresees no collision and so assists the simulated human with $\lambda = 0$. As the IAC's estimate of the simulated human's target approaches the wall, it foresees a collision and gradually increases λ to compete against the simulated human using

$$\lambda = 40\, x - 0.01\,, \quad 0 \le \lambda \le 2. \tag{49}$$

In full opposition mode at $\lambda = 2$, the IAC's reference is set to $\tau = x$, thus holding its current position. Note that when the IAC detects the estimated simulated human target going beyond the wall, the position x (thick black trace) is still far from the wall. However, the IAC's infinite horizon prediction of the future state of x foresees that it will collide with the wall, and thus competes with the human's control inputs. In comparison, the homotopy framework fails to prevent the human from hitting the wall, as it does not predict the simulated human's target. It also creates a "stiction" force that prevents the human from moving away from the wall. This is not a problem for the IAC as it detects the estimated simulated human's target moving away from the wall, updating $\lambda = 0$ to assist the simulated human in moving away. Note how in this example the transition from cooperative to competitive behaviour is gradual, yielding

a smooth interaction not offered in previous competition schemes using a virtual fixture such as [30].

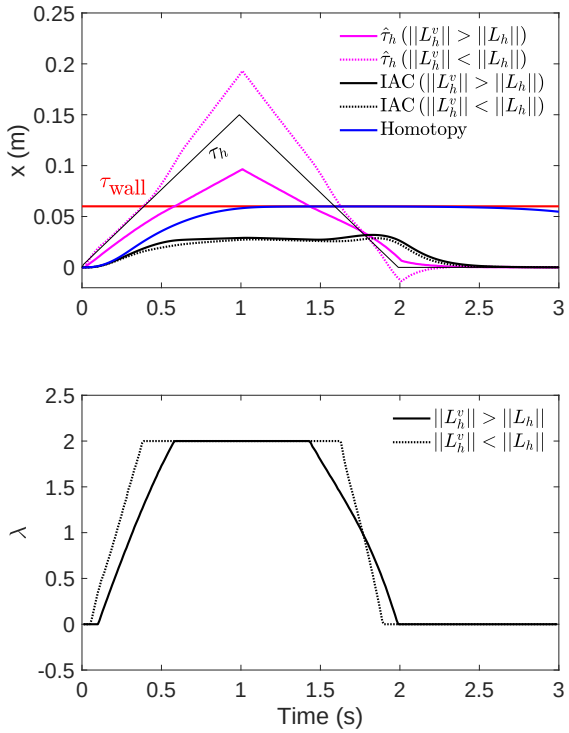

Fig. 6: Simulation of obstacle avoidance with the IAC. When the simulated human's target is far from the wall, she is assisted by the IAC, which increasingly competes as her target approaches the wall. While the estimated simulated human's target depends on whether her assumed control gains are greater (solid magenta) or smaller (dotted magenta) than they are, the IAC predicts her trajectory to avoid a collision in all cases and assists her movement when no collisions are imminent. Note how the IAC exhibits similar collision avoidance behavior even with an over- or under-estimation of the simulated human's target position. The homotopy framework fails in preventing the collision, and causes stiction when the simulated human attempts to move away from the wall.

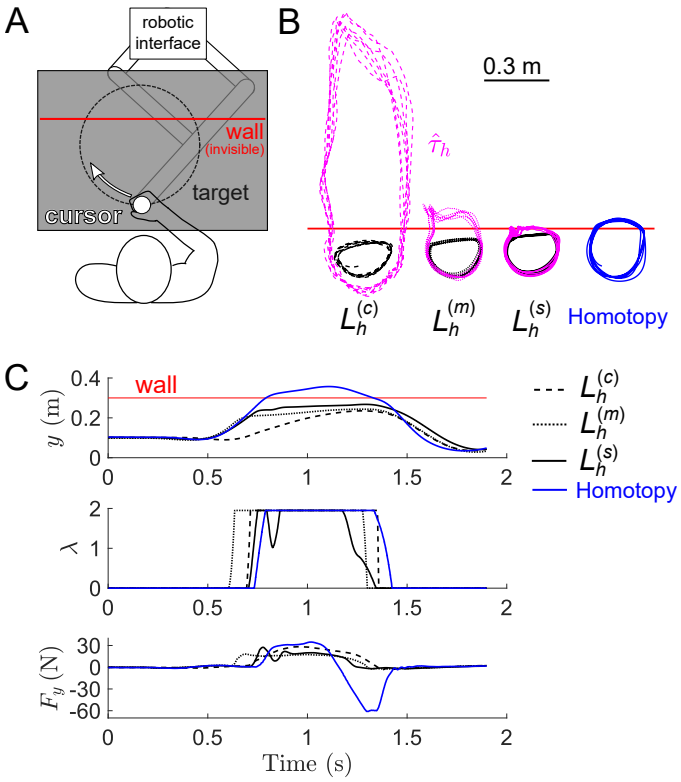

Fig. 7: Experiment demonstrating how the IAC simultaneously assists in free motion and prevents the participant from colliding into a wall (see the supplementary video) while collision and stiction occur with the homotopy framework. (A) Schematic of the tracing task with an invisible wall. (B) Sample trials from a representative participant interacting with the homotopy framework and the compliant ($L_h^{(c)}$), the medium ($L_h^{(m)}$) and the stiff IAC ($L_h^{(s)}$). Black and blue are the cursor trajectories while magenta is the estimated virtual target trajectory $\hat{\tau}_h$, which is further away from the cursor when the human gain is smaller. All IACs prevented a collision, but the homotopy framework did not. (C) y, λ and F_y from the same representative trials. λ oscillated with a stiff IAC as the virtual target oscillated around the wall. The homotopy framework exerted a stiction force that impeded the movement away from the wall.

We tested this IAC's ability to prevent a collision in an experiment. The four participants were instructed to trace a circle at constant velocity. Unknown and invisible to them was a wall positioned at $y = 0.3$ m (Figure 7A). The IAC was defined to help the participants avoid the collision with the wall by updating its target to

$$\tau = \lambda\, x + (1-\lambda)\,\hat{\tau}_h \tag{50}$$

The IAC assumed three values for the human's control gains (compliant $L_h^{(c)} \equiv [25,6]$, medium $L_h^{(m)} \equiv [100,10]$ and stiff $L_h^{(s)} \equiv [400,24]$) when estimating the human's target τ_h^v. The homotopy framework

$$\begin{aligned} u_x &= \lambda_x u_x + (1-\lambda_x u_{h_x}) \\ u_y &= \lambda_y u_y + (1-\lambda_y u_{h_y}) \end{aligned} \tag{51}$$

was implemented alongside the three IACs, where λ_x and λ_y was updated according to

$$\begin{aligned} \lambda_x &= 0 \\ \lambda_y &= 40y - 10,\ \ 0 \le \lambda_y \le 2 \end{aligned} \tag{52}$$

The participants traced the circle for 4 blocks, each with 5 trials to test out the different IACs and the homotopy framework.

The virtual target was further away from the cursor's trajectory and penetrated deeper into the wall when the human's control gains were smaller (Figure 7B). The homotopy framework could not prevent the participant from colliding into the wall, and it also exerted a stiction force that impeded the participant from moving away from it (Figure 7C). λ_y oscillated with the stiff IAC as the virtual

target, which was close to the cursor's trajectory, moved in and out of the wall.

6 Discussion

This paper has introduced an Intention Assimilation Controller (IAC) to shape the physical interaction between a contact robot and a human. The IAC lets the robot estimate the human's motion plan, and considers it to control the common movement according to task's requirements and a desired interaction strategy. In experiments, we showed that the IAC can assist the human's movement, reducing the effort they exerted in the tracing task, to a level comparable to the homotopy framework [33]. However, the homotopy framework failed to prevent the human from colliding into a virtual wall, in contrast with the IAC, which stopped the collision. The assistance was similar between the IAC and the homotopy framework because both controllers exert the measured human's force under full assistance mode. However, the IAC can oppose the human's force while the homotopy framework cannot, which is why the latter is not suitable for collision avoidance.

Different from the existing methods [22], [23], [24], [25], [26], the IAC's efficiency does not rely on an accurate estimate of the human's control, which can hardly be identified on simple trajectories [10], [38] or require assumptions about the human model or their movement. Instead, the IAC assumes *a priori* control gains for the human, and uses them to identify the human's putative motion target. This "virtual target" can then be combined with the task's goal, in a continuum of desired interaction strategies, from collaboration to independent co-activity and antagonistic competition.

While previous works have developed pragmatic human-robot interaction strategies e.g. [13], [15], [23], [50], we decided to develop the IAC using a strict control scheme. This enabled us to show that the IAC induces a stable interaction, independently on the assumed control gains for the human, thus demonstrating the safety and validity of this approach. The simulations and experiments of this paper illustrated the versatility of the IAC framework, that can be used to implement various tasks, including reaching (Figures 3, 4), tracing/tracking (Figures 5, 7), and obstacle avoidance (Figures 6, 7). As the IAC relies on the prediction of the human's target trajectory (not merely on their current state as in [33]) to determine its behaviour, it can provide motion guidance with less force, and safer obstacle avoidance than previous approaches, as was demonstrated in the simulation and experiment results.

Using the IAC the designer can tailor the assumed control gains depending on the specific application. An IAC with small control gains yields a soft interaction and is conservative in operation as it foresees collisions. An IAC with large control gains should be used in enclosed spaces like in robot-assisted surgery where the IAC can assist the surgeon to pass through small openings but avoid hitting the sides. In this case, a near future prediction of the intended motion is more useful in discriminating plausible collisions. The control gains might also be identified using task performance based reinforcement learning to identify optimal control gains for a specific task.

The IAC provides a continuum of interaction strategies from assistance to competition not available in previous schemes. While earlier literature focused on a leader-follower paradigm [27], [28], [32], other interaction behaviors were also investigated in the literature [7], [33], [37], [42], [43]. A standard leader-follower paradigm failed to assist the human and cannot impose antagonistic behavior for collision avoidance. Antagonistic behaviors have been provided previously as e.g. virtual fixtures [30], but these schemes do not possess a mechanism to continuously adapt the robot's interaction behavior. The homotopy framework [33] can assist the human, but as it modifies the human-robot interaction by using the human's force, it could not prevent an imminent collision. Additionally, the simulation and experiment of Figures 5, 7 showed that the homotopy framework has the unintended consequence of antagonising the human when they move away from the wall. In contrast, the IAC estimates the human's motion intention in the near future, understanding whether the human will collide into a wall or if s/he is attempting to move away from it. This distinction is critical to employing antagonistic or assistive behavior at the right moment. Such decision-making requires the human's motion intention and knowledge of the surroundings.

The IAC's ability to estimate the human's intention to modify the human-robot interaction can be critical to applications in physical rehabilitation, robot-assisted surgery and shared driving. Using information about the environment, the IAC can estimate the human's intended motion and tune the physical interaction correspondingly, smoothly transitioning from assistive to antagonistic behavior, e.g. when the driver is turning a corner too aggressively in shared driving. However, it is unclear what level of assistive or antagonistic behavior is acceptable during operation, and how a human may react to the robot's intervention. User experience studies should be conducted to find the acceptable level, which may be task dependent.

References

[1] R. H. Taylor, A. Menciassi, G. Fichtinger, P. Fiorini, and P. Dario, *Medical Robotics and Computer-Integrated Surgery*, pp. 1657–1684. Cham: Springer International Publishing, 2016.

[2] M. Semprini, M. Laffranchi, V. Sanguineti, L. Avanzino, R. De Icco, L. De Michieli, and M. Chiappalone, "Technological approaches for neurorehabilitation: From robotic devices to brain stimulation and beyond," *Frontiers in Neurology*, vol. 9, p. 212, 2018.

[3] A. Ajoudani, A. M. Zanchettin, S. Ivaldi, A. Albu-Schäffer, K. Kosuge, and O. Khatib, "Progress and prospects of the human-robot collaboration," *Autonomous Robots*, vol. 42, pp. 957–975, Jun 2018.

[4] K. Reed, M. Peshkin, M. Hartmann, J. Patton, P. Vishton, and M. Grabowecky, "Haptic cooperation between people, and between people and machines," in *Intelligent Robots and Systems, 2006 IEEE/RSJ International Conference on*, pp. 2109 –2114, Oct. 2006.

[5] K. Reed, J. Patton, and M. Peshkin, "Replicating Human-Human Physical Interaction," in *Robotics and Automation, 2007 IEEE International Conference on*, pp. 3615 –3620, Apr. 2007.

[6] A. Kucukyilmaz, T. Sezgin, and C. Basdogan, "Conveying intentions through haptics in human-computer collaboration," in *World Haptics Conference (WHC), 2011 IEEE*, pp. 421 –426, June 2011.

[7] A. Mörtl, M. Lawitzky, A. Kucukyilmaz, M. Sezgin, C. Basdogan, and S. Hirche, "The role of roles: Physical cooperation between humans and robots," *The International Journal of Robotics Research*, vol. 31, pp. 1656–1674, Nov. 2012.

[8] R. Groten, D. Feth, R. L. Klatzky, and A. Peer, "The role of haptic feedback for the integration of intentions in shared task execution," *IEEE Transactions on Haptics*, vol. 6, no. 1, pp. 94–105, 2013.

[9] C. E. Madan, A. Kucukyilmaz, T. M. Sezgin, and C. Basdogan, "Recognition of haptic interaction patterns in dyadic joint object manipulation," *IEEE Transactions on Haptics*, vol. 8, no. 1, pp. 54–66, 2015.

[10] A. Takagi, N. Beckers, and E. Burdet, "Motion plan changes predictably in dyadic reaching," *PLOS ONE*, vol. 11, p. e0167314, Dec. 2016.

[11] K. Mojtahedi, B. Whitsell, P. Artemiadis, and M. Santello, "Communication and inference of intended movement direction during human–human physical interaction," *Frontiers in Neurorobotics*, vol. 11, p. 21, 2017.

[12] A. Takagi, G. Ganesh, T. Yoshioka, M. Kawato, and E. Burdet, "Physically interacting individuals estimate the partner's goal to enhance their movements," *Nature Human Behaviour*, vol. 1, p. 0054, Mar. 2017.

[13] D. P. Losey, C. G. McDonald, E. Battaglia, and M. K. O'Malley, "A Review of Intent Detection, Arbitration, and Communication Aspects of Shared Control for Physical Human-Robot Interaction," *Applied Mechanics Reviews*, vol. 70, pp. 010804–010804–19, Feb. 2018.

[14] A. Bussy, P. Gergondet, A. Kheddar, F. Keith, and A. Crosnier, "Proactive behavior of a humanoid robot in a haptic transportation task with a human partner," in *2012 IEEE RO-MAN: The 21st IEEE International Symposium on Robot and Human Interactive Communication*, pp. 962–967, 2012.

[15] K. Wakita, J. Huang, P. Di, K. Sekiyama, and T. Fukuda, "Human-Walking-Intention-Based Motion Control of an Omnidirectional-Type Cane Robot," *IEEE/ASME Transactions on Mechatronics*, vol. 18, pp. 285–296, Feb. 2013.

[16] W. Takano, T. Jodan, and Y. Nakamura, "Recursive process of motion recognition and generation for action-based interaction," *Advanced Robotics*, vol. 29, no. 4, pp. 287–299, 2015.

[17] J. Lanini, H. Razavi, J. Urain, and A. Ijspeert, "Human intention detection as a multiclass classification problem: Application in physical human–robot interaction while walking," *IEEE Robotics and Automation Letters*, vol. 3, no. 4, pp. 4171–4178, 2018.

[18] S. Javdani, H. Admoni, S. Pellegrinelli, S. S. Srinivasa, and J. A. Bagnell, "Shared autonomy via hindsight optimization for teleoperation and teaming," *The International Journal of Robotics Research*, vol. 37, no. 7, pp. 717–742, 2018.

[19] K. Hauser, "Recognition, prediction, and planning for assisted teleoperation of freeform tasks," *Autonomous Robots*, vol. 35, 11 2013.

[20] E. Berger, D. Vogt, N. Haji-Ghassemi, B. Jung, and H. B. Amor, "Inferring guidance information in cooperative human-robot tasks," in *2013 13th IEEE-RAS International Conference on Humanoid Robots (Humanoids)*, pp. 124–129, 2013.

[21] E. Noohi, M. Žefran, and J. L. Patton, "A Model for Human #x2013;Human Collaborative Object Manipulation and Its Application to Human #x2013;Robot Interaction," *IEEE Transactions on Robotics*, vol. 32, pp. 880–896, Aug. 2016.

[22] Y. Maeda, T. Hara, and T. Arai, "Human-robot cooperative manipulation with motion estimation," in *Proceedings 2001 IEEE/RSJ International Conference on Intelligent Robots and Systems. Expanding the Societal Role of Robotics in the the Next Millennium (Cat. No.01CH37180)*, vol. 4, pp. 2240–2245 vol.4, 2001.

[23] B. Corteville, E. Aertbelien, H. Bruyninckx, J. D. Schutter, and H. V. Brussel, "Human-inspired robot assistant for fast point-to-point movements," in *Proceedings 2007 IEEE International Conference on Robotics and Automation*, pp. 3639–3644, Apr. 2007.

[24] A. Thobbi, Y. Gu, and W. Sheng, "Using human motion estimation for human-robot cooperative manipulation," in *2011 IEEE/RSJ International Conference on Intelligent Robots and Systems*, pp. 2873–2878, 2011.

[25] S. S. Ge, Yanan Li, and Hongsheng He, "Neural-network-based human intention estimation for physical human-robot interaction," in *2011 8th International Conference on Ubiquitous Robots and Ambient Intelligence (URAI)*, pp. 390–395, 2011.

[26] J. R. Medina, T. Lorenz, and S. Hirche, "Synthesizing anticipatory haptic assistance considering human behavior uncertainty," *IEEE Transactions on Robotics*, vol. 31, no. 1, pp. 180–190, 2015.

[27] V. Duchaine and C. M. Gosselin, "General model of human-robot cooperation using a novel velocity based variable impedance control," in *Second Joint EuroHaptics Conference and Symposium on Haptic Interfaces for Virtual Environment and Teleoperator Systems (WHC'07)*, pp. 446–451, 2007.

[28] F. Ficuciello, L. Villani, and B. Siciliano, "Variable impedance control of redundant manipulators for intuitive human–robot physical interaction," *IEEE Transactions on Robotics*, vol. 31, no. 4, pp. 850–863, 2015.

[29] V. Villani, F. Pini, F. Leali, and C. Secchi, "Survey on human-robot collaboration in industrial settings: Safety, intuitive interfaces and applications," *Mechatronics*, vol. 55, pp. 248–266, Nov. 2018.

[30] T. Xia, A. Kapoor, P. Kazanzides, and R. Taylor, "A constrained optimization approach to virtual fixtures for multi-robot collaborative teleoperation," in *2011 IEEE/RSJ International Conference on Intelligent Robots and Systems*, pp. 639–644, 2011.

[31] F. Abdollahi, E. D. Case Lazarro, M. Listenberger, R. V. Kenyon, M. Kovic, R. A. Bogey, D. Hedeker, B. D. Jovanovic, and J. L. Patton, "Error Augmentation Enhancing Arm Recovery in Individuals With Chronic Stroke: A Randomized Crossover Design," *Neurorehabilitation and Neural Repair*, vol. 28, pp. 120–128, Feb. 2014.

[32] Y. Karayiannidis, C. Smith, and D. Kragic, "Mapping human intentions to robot motions via physical interaction through a jointly-held object," in *The 23rd IEEE International Symposium on Robot and Human Interactive Communication*, pp. 391–397, 2014.

[33] P. Evrard and A. Kheddar, "Homotopy switching model for dyad haptic interaction in physical collaborative tasks," in *EuroHaptics conference, 2009 and Symposium on Haptic Interfaces for Virtual Environment and Teleoperator Systems. World Haptics 2009. Third Joint*, pp. 45–50, Mar. 2009.

[34] A. Enes and W. Book, "Blended shared control of zermelo's navigation problem," in *Proceedings of the 2010 American Control Conference*, pp. 4307–4312, 2010.

[35] P. Leica, J. M. Toibero, F. Roberti, and R. Carelli, "Bilateral human-robot interaction with physical contact," in *2013 16th International Conference on Advanced Robotics (ICAR)*, pp. 1–6, 2013.

[36] Y. Li, K. P. Tee, W. L. Chan, R. Yan, Y. Chua, and D. K. Limbu, "Continuous Role Adaptation for Human #x2013;Robot Shared Control," *IEEE Transactions on Robotics*, vol. 31, pp. 672–681, June 2015.

[37] Y. Li, K. P. Tee, R. Yan, W. L. Chan, and Y. Wu, "A framework of human-robot coordination based on game theory and policy iteration," *IEEE Transactions on Robotics*, vol. 32, pp. 1408–1418, Dec 2016.

[38] Y. Li, G. Carboni, F. Gonzalez, D. Campolo, and E. Burdet, "Differential game theory for versatile physical human-robot interaction," *Nature Machine Intelligence*, vol. 1, p. 36, Jan. 2019.

[39] N. Jarrassé, T. Charalambous, and E. Burdet, "A framework to describe, analyze and generate interactive motor behaviors," *PLoS ONE*, vol. 7, p. e49945, Nov. 2012.

[40] N. Jarrassé, V. Sanguineti, and E. Burdet, "Slaves no longer: review on role assignment for human-robot joint motor action," *Adaptive Behavior*, vol. 22, no. 1, pp. 70–82, 2014.

[41] M. Laghi, M. Maimeri, M. Marchand, C. Leparoux, M. Catalano, A. Ajoudani, and A. Bicchi, "Shared-autonomy control for intuitive bimanual tele-manipulation," in *2018 IEEE-RAS 18th International Conference on Humanoid Robots (Humanoids)*, pp. 1–9, 2018.

[42] M. S. Erden and T. Tomiyama, "Human-Intent Detection and Physically Interactive Control of a Robot Without Force Sensors," *IEEE Transactions on Robotics*, vol. 26, pp. 370–382, Apr. 2010.

[43] E. Gribovskaya, A. Kheddar, and A. Billard, "Motion learning and adaptive impedance for robot control during physical interaction with humans," in *2011 IEEE International Conference on Robotics and Automation*, pp. 4326–4332, May 2011.

[44] J. J. Craig, *Introduction to Robotics: Mechanics and Control*. Boston, MA, USA: Addison-Wesley Longman Publishing Co., Inc., 2nd ed., 1989.

[45] N. Hogan, "Impedance control: An approach to manipulation," *Journal of Dynamic Systems, Measurement and Control, Transactions of the ASME*, vol. 107, no. 1, pp. 1–24, 1985.

[46] P. Tomei, "Adaptive PD controller for robot manipulators," *IEEE Transactions on Robotics and Automation*, vol. 7, pp. 565–570, Aug. 1991.

[47] G. F. Franklin, J. D. Powell, and A. Emami-Naeini, *Feedback Control of Dynamic Systems*. Upper Saddle River, NJ, USA: Prentice Hall Press, 7th ed., 2014.

[48] K. Astrom and B. Wittenmark, *Adaptive control*. Reading: MA: Addison-Wesley, 1995.

[49] E. Burdet, D. W. Franklin, and T. E. Milner, *Human Robotics: Neuromechanics and Motor Control*. MIT Press, Sept. 2013.
[50] C. Huang, G. Wasson, M. Alwan, P. Sheth, and R. Ledoux, "Shared Navigational Control and User Intent Detection in an Intelligent Walker," *AAAI Fall 2005 Symposium*, Nov. 2005.

Atsushi Takagi (S'13-M'15) received the MS degree in physics and the PhD degree in computational neuroscience from Imperial College London, United Kingdom. He is a Distinguished Researcher at NTT Communication Science Laboratories, mainly interested in motor control, using a mix of behavioral experiments and computational modelling. This knowledge is applied to human-human and human-robot interaction.

Yanan Li (S'10-M'14) received the BEng and MEng degrees from the Harbin Institute of Technology, China, in 2006 and 2008, respectively, and the PhD degree from the National University of Singapore, in 2013. Currently he is a Lecturer in Control Engineering with the Department of Engineering and Design, University of Sussex, UK. From 2015 to 2017, he has been a Research Associate with the Department of Bioengineering, Imperial College London, UK. From 2013 to 2015, he has been a Research Scientist with the Institute for Infocomm Research (I2R), Agency for Science, Technology and Research (A*STAR), Singapore. His general research interests include physical human-robot interaction, human-robot collaboration, and control theory and applications.

Etienne Burdet (S'92-M'96) received the MS degree in mathematics, the MS degree in physics, and the PhD degree in robotics, all from ETH-Zurich, Switzerland. He is Professor and Chair in Human Robotics at Imperial College London, and his main research interest is in human-machine interaction. He uses an integrative approach of neuroscience and robotics to investigate human sensorimotor control, and to design efficient assistive devices and training systems for neuro-rehabilitation, which are tested in clinical trials and commercialized.